Spatially Noiseless Optical Amplification of Images

Alexis Mosset, Fabrice Devaux, and Eric Lantz*

Institut FEMTO-ST, Laboratoire d'Optique PM Duffieux, UMR CNRS/Université de Franche-Comté 6174, 25030 Besançon CEDEX, France†

(Received 24 November 2004; published 9 June 2005)

We present the first experimental demonstration of noiseless amplification of images, where noise refers to spatial quantum fluctuations on the pixels of single shot images. Phase-sensitive and phase-insensitive schemes are compared and the noise figures are in good agreement with theory, inasmuch this theory includes the quantum efficiency of the whole system and the pixel size.

DOI: 10.1103/PhysRevLett.94.223603 PACS numbers: 42.50.Lc, 42.50.Ar, 42.65.Yj

A phase-sensitive amplifier (PSA) can be used to amplify light limited by shot noise without degrading the signal-to-noise ratio (SN), while a phase-insensitive amplifier (PIA) adds 3 dB of noise [1]. Noiseless optical parametric amplification was experimentally demonstrated about ten years ago for a single mode beam [2]. More recently, reducing quantum fluctuations of light in imaging systems has attracted considerable interest to obtain noiseless image amplification [3–5], image entanglement [6,7], or generation of multimode squeezing [8,9]. However, most of these studies considered only temporal fluctuations which affect a spatial pattern. Regarding parametric amplification, the experiment in the Kumar's group [3] showed that a phase-sensitive scheme allows the signal-to-noise ratio to be unmodified over an entire image, where the noise is recorded at a frequency of 27 MHz by a photodiode. As the photodiode scanned the image, this result proves that phase-sensitive amplification improves the regularity in time of the distribution of photons for each point of the image, but, because only fluctuations in the time domain were recorded, it does not directly show a regularity in space. However, patterns in an image are pure spatial information, without any time aspect, that are ultimately degraded by spatial fluctuations of quantum origin for very weak images. Fluctuations in quantum mechanics are described by ensemble averages, which are often estimated by time averages if the signal is stationary in time, but which can also be estimated by spatial averages if the signal is stationary in space on a sufficiently large area. For spontaneous down-conversion, the distribution of such spatial fluctuations on single shot images has been characterized [10] and sub-shot-noise signal-idler correlations have been demonstrated [11]. In this Letter, we report the first experimental observation of noiseless amplification of images by a phase-sensitive optical parametric amplifier, where noise refers to pure spatial fluctuations on single shot images, and we compare the results with the PIA scheme.

The quantum noise properties of an optical parametric amplifier (OPA) are described by the noise figure $\mathrm{NF} = \mathrm{SN}_{\mathrm{in}}/\mathrm{SN}_{\mathrm{out}}$. However, if $\mathrm{SN}_{\mathrm{out}}$ is the output signal-to-noise ratio after detection with a quantum efficiency $\eta < 1$, the input signal-to-noise ratio $\mathrm{SN}_{\mathrm{in}}$ of a Poissonian beam is not a directly measurable quantity. What can be effectively measured is the SN after detection without amplification, resulting in multiplying both the input SN and the noise figure by the global quantum efficiency of the system η_{tot}. Unlike the ''theoretical'' noise figure NF, the practical ratio $R = \eta_{\mathrm{tot}} \times \mathrm{NF}$ can be smaller than 1, meaning that the amplified image is less degraded by the detection than the shot noise limited input [12]. Indeed, the ideal noiseless squeezing transformation performed by a PSA induces bunching of photons when the amplitude quadrature is amplified. Because of its intrinsic redundancy, such a super-Poissonian image is less degraded than a Poissonian image by a poor detector quantum efficiency. In the PIA case, such a property remains valid at the detection stage, but vacuum fluctuations enter the idler unused port [1], resulting in a 3 dB degradation of the NF. R is given in the PSA and PIA schemes as [2]

$$R_{\mathrm{PSA}} = \eta_{\mathrm{tot}}\left[1 - \frac{1}{G_{\mathrm{PSA}}} + \frac{1}{\eta_{\mathrm{tot}} G_{\mathrm{PSA}}}\right], \tag{1}$$

where G_{PSA} is the phase-sensitive gain of the OPA, and

$$R_{\mathrm{PIA}} = \eta_{\mathrm{tot}}\left[2 - \frac{2}{G_{\mathrm{PIA}}} + \frac{1}{\eta_{\mathrm{tot}} G_{\mathrm{PIA}}}\right], \tag{2}$$

where G_{PIA} is the phase-insensitive gain of the OPA. Moreover, Sokolov *et al.* [5] have shown that using a detector with a pixel size S_d much smaller than the coherence area S_{diff} in the amplified image is equivalent to multiply the quantum efficiency by the ratio S_d/S_{diff} in Eqs. (1) and (2). It means physically that, even for a strongly multimode beam, detecting only a part of one of these spatial modes is equivalent to introduce losses, as for a monomode beam. Note that such degradation of the SN due to too small pixels can be effectively overcome by the amplification if we consider temporal fluctuations while this improvement is an artefact for spatial signals, because the OPA itself rejects both signal and noise of high spatial frequencies [13]. Nevertheless, the influence of the pixel size on the noise figure is strong for spatial as well for temporal fluctuations and this Letter is the first, to the best

of our knowledge, to show experimentally this influence in image amplification.

The experimental setup is a traveling-wave OPA similar to that described in [14]. The signal and pump pulses are provided, respectively, by the second harmonic [1.2 ps duration (FWHM) at 527.5 nm] and the fourth harmonic (0.93 ps duration at 263.7 nm) of a Q-switched mode-locked Nd:Glass laser (twinkle laser by light conversion) at a repetition rate of 33 Hz. The amplification is performed in a beta-barium-borate (BBO) crystal whose transverse area, $7 \times 7\ \mathrm{mm}^2$, is chosen in order to obtain a sufficient number of resolution cells in the amplified image so as to perform valid statistics. The crystal length, 4 mm, is limited by the group-velocity difference between the UV pump and the green signal. Because of the high dispersion of the crystal in the UV, only type 1 amplification is possible for this couple of wavelengths. Hence, collinear interaction is phase sensitive, while phase-insensitive amplification is obtained by a slight angular shift between the pump and signal beams, as shown in Fig. 1. The signal beam, whose intensity can be precisely controlled by means of densities, a half-wave plate, and a Glan polarizer, is widened by a telescope and illuminates a resolution chart. A line of this chart is imaged on the input face of the crystal by a second telescope and then onto the CCD camera by the lens L. The CCD camera includes a back-illuminated thin silicon array, cooled at $-40\,^{\circ}\mathrm{C}$ with a pixel area of $20 \times 20\ \mu\mathrm{m}^2$, a negligible dark current of $0.03\ e^-\ \mathrm{pix}^{-1}\,\mathrm{s}^-$, and a readout noise around $3.2\ e^-$ rms measured on a nonilluminated part of the array. To match the phase fronts, the beam waists of the signal and the pump are superimposed within the crystal. A filtering hole, placed in the Fourier plane and centered around the zero spatial frequency of the signal image, limits the detected intensity of spontaneous down-conversion (SPDC) and ensures the elimination of the idler in the PIA scheme. However, the spatial spectral bandwidth in the detected image is reduced by this hole and, in practice, the size of S_{diff} is no longer determined by the phase-matching conditions but rather by the diameter $D = 0.5$ mm of the hole,

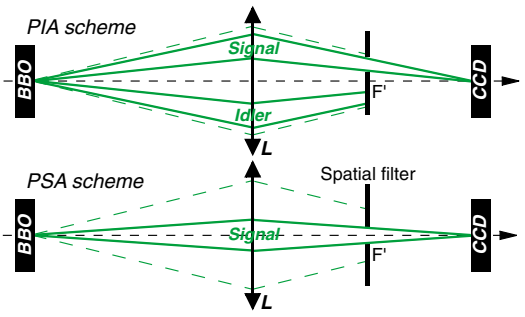

FIG. 1 (color online). Phase-matching conditions. Top: Noncollinear for PIA scheme. Bottom: Collinear for PSA scheme. Green or gray dashed lines: Spatial spectral bandwidth of OPA. Solid line: Resolution range.

giving a maximum spatial frequency $u_{\mathrm{max}} \simeq 5.9\ \mathrm{mm}^{-1}$. From u_{max}, we calculate a number of 41×41 amplified resolution cells in the crystal. With a 0.86 magnification, the transverse size of S_{diff} is 7.3 pixels on the camera. In the following, the results will be presented for different groupings of the pixels (achieved by software) in order to consider effective detector areas S_d smaller or greater than S_{diff}. The NF depends on the resulting total quantum efficiency η_{tot} that can be computed as the product of the quantum efficiency (η_{CCD}) of the CCD camera by the transmission (η_{opt}) of the optical elements after the crystal:

$$\eta_{\mathrm{tot}} = \eta_{\mathrm{opt}} \times \eta_{\mathrm{CCD}} = 0.69 \times 0.9 = 0.62 \pm 0.10. \quad (3)$$

The uncertainty comes from the evaluation of η_{opt}, while η_{CCD} is given by the manufacturer. The experimental procedure to measure R is achieved in three main steps that are identical in the PIA and PSA schemes. The first step consists in measuring SN without amplification (i.e., $\eta_{\mathrm{tot}}\mathrm{SN}_{\mathrm{in}}$) along with a statistical verification of the Poissonian hypothesis. In the second step, the intensity of the SPDC is measured and its level is subtracted from the amplified images. The third step consists of measuring $\mathrm{SN}_{\mathrm{out}}$.

For the first step, the shot-to-shot stability of the laser is sufficient to estimate the level of the input images by recording a set of about 20 nonamplified images. Two sets with different intensity levels were recorded in the PIA scheme. For each set, we have verified that a nongrouped image is well described by a Poissonian distribution, while grouping degrades this distribution because of residual deterministic defects. Nevertheless, the experimental statistics on the difference between two images of a set remains Poissonian because the subtraction of images eliminates deterministic structures [15]:

$$\eta_{\mathrm{tot}}\mathrm{SN}_{\mathrm{in}} = \overline{n}_p \times S_d = \overline{n}, \quad (4)$$

where S_d is the detector area after grouping, expressed in pixels. In Eq. (4) and in all the following, $\overline{n}_p$ is the mean number of photoelectrons per pixel, while n designates the number of photoelectrons on S_d, obtained by summing the gray levels on the pixels and multiplying by the appropriate scaling factor.

To estimate the SPDC level, 20 images were recorded by injecting only the pump. Because type 1 phase matching is noncritical in wavelength [16], the SPDC is strongly temporally multimode. These modes add incoherently while each temporal mode is described by a thermal statistic [10]. The number of temporal modes are experimentally assessed as

$$M_t = \frac{(\overline{n}_p^{\mathrm{SPDC}}/\eta_{\mathrm{tot}}) \times S_{\mathrm{diff}}}{G - 1}, \quad (5)$$

where $\overline{n}_p^{\mathrm{SPDC}}$ is the mean level of SPDC per pixel before grouping and G the gain of the OPA. Consequently, the variance of the SPDC on a grouped pixel is given by

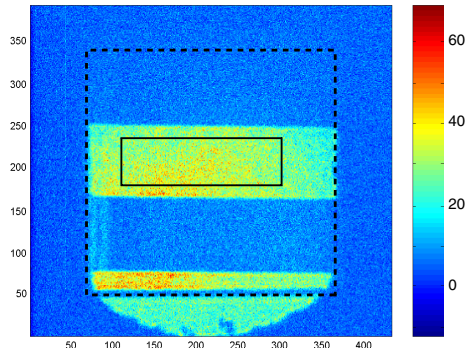

FIG. 2 (color online). Example of amplified image in the PIA scheme. Dashed line: Edges of the crystal. Solid line: Limits of the area used for the statistics (8241 pixels).

$$(\overline{\Delta n^2}_{\mathrm{SPDC}}) = \frac{(\overline{n}_{\mathrm{SPDC}})^2}{M_t} + \overline{n}_{\mathrm{SPDC}}, \tag{6}$$

where the first term on the right-hand side of Eq. (6) describes the classical fluctuations and the second term the shot noise. Equation (6) does not take into account deterministic variations of SPDC due to, for example, imperfections of the pump profile, which are not negligible for large grouping when directly measuring the SPDC variance. Because these variations do not affect difference images, we use Eq. (6) rather than a direct measurement to calculate the SPDC variance.

The measurement of $\mathrm{SN}_{\mathrm{out}}$ is performed by using single shot images, in order to take into account the strong variations of the gain from one shot to another in the phase-sensitive scheme because of the noncontrolled variations of the relative phase between the signal and the pump. Such a control is made difficult by the low repetition rate of both the laser source (33 Hz) and the camera (< 1 Hz). Classical noise is predominant in the amplified images because of deterministic imperfections of the system (pump beam, lenses, etc.), and good results have been obtained only by performing differences of images, in order to eliminate the spatial defects that are reproducible from one shot to another. $\mathrm{SN}_{\mathrm{out}}$ is measured as follows. First, an area where the mean intensity is as constant as possible is selected in the amplified image. Second, the measurement of SN on all amplified images without subtraction allows the selection of images with the highest SNs. Third, pairs of images are defined by all permutations between the selected images. Fourth, the mean and the variance are calculated as follows for each pair and each grouping. The mean is calculated as the mean of the two images corrected by subtracting the electronic background $\overline{n}_{glb}$ and converted in photoelectrons (pe^-). Last, the mean of the SPDC is subtracted. The whole calculation is summarized in Eq. (7):

$$\overline{n} = g_{\acute{e}} \times (\overline{n}_{gl} - \overline{n}_{glb}) - (\overline{n}_{\mathrm{SPDC}}), \tag{7}$$

where $g_{\acute{e}} = 0.97\ pe^- \cdot \mathrm{gl}^{-1}$ converts gray level (gl) in pe^-. The variance in the amplified image is computed as half the variance of the difference of the images, with subtraction of the variances of the readout noise $(\overline{\Delta n^2}_{\mathrm{subread}})$ and of the SPDC:

$$\overline{\Delta n^2} = \frac{1}{2} \times \{[(\overline{\Delta n^2}_{\mathrm{sub}}) - (\overline{\Delta n^2}_{\mathrm{subread}})] - 2 \times (\overline{\Delta n^2}_{\mathrm{SPDC}})\}. \tag{8}$$

$\mathrm{SN}_{\mathrm{out}}$ is computed for each value of the detector area as

$$\mathrm{SN}_{\mathrm{out}} = \frac{(\overline{n})^2}{(\overline{\Delta n^2})}. \tag{9}$$

From this value and the corresponding value $\eta_{\mathrm{tot}}\mathrm{SN}_{\mathrm{in}}$, the ratio R is determined for each pair of images and the mean ratio is assessed from all pairs. The experimental error bars are finally determined as twice the standard deviation divided by the square root of the number of pairs of selected images.

In the PIA scheme, about 100 amplified images were recorded for each set of nonamplified images and the gain

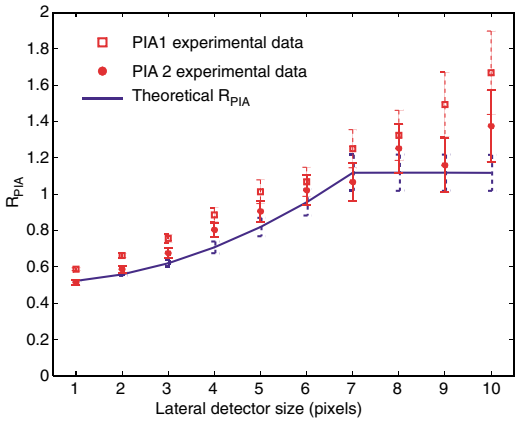

FIG. 3 (color online). NF after detection in the PIA scheme versus the detector size. Squares: Experimental data of PIA series 1 (dotted error bars). Circles: Experimental data of PIA series 2 (solid line error bars). Line: Theoretical curve (heavy dotted error bars).

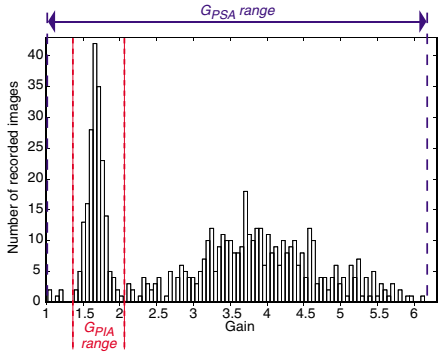

FIG. 4 (color online). Histogram of the gain for both the PIA and PSA schemes.

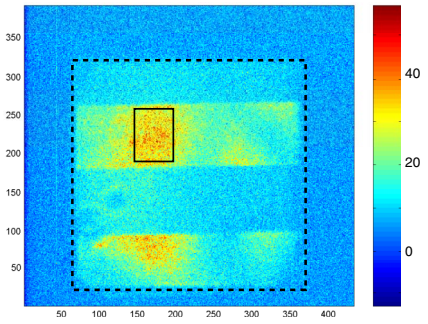

FIG. 5 (color online). Example of an amplified image in the PSA scheme. Area of 3266 pixels.

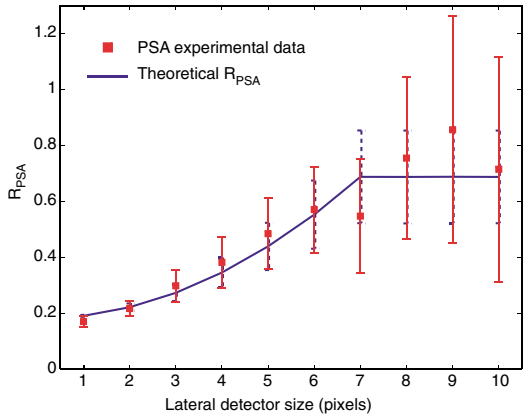

FIG. 6 (color online). NF after detection in the PSA scheme versus the lateral detector size. Squares: Experimental data (solid line error bars). Line: Theoretical curve (heavy dotted error bars).

was estimated for each image from the mean in the corresponding set of nonamplified images. The gain variations are due to the shot-to-shot fluctuations of the laser. The average gain is $G_{\mathrm{PIA}} = 1.6 \pm 0.5$. Ten images have been selected with a constant gain for each set. Figure 2 shows an example of a selected image. Figure 3 reports the NF after detection for the PIA scheme versus the detector size. For $S_d \geq S_{\mathrm{diff}}$, the theoretical R is $R_{\mathrm{PIA}} = 1.1 \pm 0.1$. For $S_d < S_{\mathrm{diff}}$, we use $\eta_{\mathrm{tot}} \times (S_d/S_{\mathrm{diff}})$ in Eq. (2), although this assumption is only correct when $S_d \ll S_{\mathrm{diff}}$, as explained previously. The uncertainty is defined by the uncertainty on η_{tot} given in Eq. (3). The experimental data and the theoretical curve are in good agreement. The differences between the two sets, realized in equivalent conditions, remain in the uncertainty range due to the random character of fluctuations

In the PSA scheme, about 500 images were recorded and the gain was measured for each image with a range from 1 to 6, as shown in Fig. 4. Because the relative phase is not controlled, it is more difficult to find pairs of images that correspond both to the same (maximum) gain and the same phase. Nevertheless, the criteria based on the highest SN allow the selection of five images which were amplified in the same conditions. Figure 5 shows an example of a selected image. The gain is clearly nonhomogeneous along the line because of residual variations of the relative phase. Therefore the used area where the statistics can be assumed as stationary is smaller than in the PIA case. The gains of the selected images are among the highest with the following average value: $G_{\mathrm{PSA}} = 5.6 \pm 0.5$. Figure 6 shows the evolution of the NF after detection for the PSA scheme versus the detector size. The theoretical curve is calculated from Eq. (1) as in the PIA scheme, giving $R_{\mathrm{PSA}} = 0.7 \pm 0.1$ when $S_d \geq S_{\mathrm{diff}}$. The agreement between experimental data and theoretical curve is good and proves the noiseless character of the PSA scheme.

In conclusion, we have reported the first experimental observation of purely spatial noiseless amplification of images by a PSA scheme and we have compared the results with the PIA scheme. The obtained results are in satisfactory agreement with theory, for a sufficient number of independent pixels: more than a hundred for the greatest grouping. As expected, the PSA does not add noise, while PIA leads to the expected 3 dB degradation of the SN.

This work was supported by the E.U. in the frame of the QUANTIM network (Contract No. IST 2000-26019).

*Electronic address: elantz@univ-fcomte.fr
†Electronic address: http://lopmd.univ-fcomte.fr/onl

[1] C. M. Caves, Phys. Rev. D **26**, 1817 (1982).
[2] J. A. Levenson, I. Abram, T. Rivera, and P. Grangier, J. Opt. Soc. Am. B **10**, 2233 (1993).
[3] S.-K. Choi, M. Vasilyev, and P. Kumar, Phys. Rev. Lett. **83**, 1938 (1999).
[4] M. I. Kolobov and L. A. Lugiato, Phys. Rev. A **52**, 4930 (1995).
[5] I. V. Sokolov, M. I. Kolobov, and L. A. Lugiato, Phys. Rev. A **60**, 2420 (1999).
[6] A. Gatti, E. Brambilla, L. A. Lugiato, and M. Kolobov, Phys. Rev. Lett. **83**, 1763 (1999).
[7] T. B. Pittman, D. V. Strekalov, D. N. Klyshko, M. H. Rubin, A. V. Sergienko, and Y. H. Shih, Phys. Rev. A **53**, 2804 (1996).
[8] M. I. Kolobov and I. V. Sokolov, Sov. Phys. JETP **69**, 1097 (1989).
[9] M. I. Kolobov, Rev. Mod. Phys. **71**, 1539 (1999).
[10] A. Mosset, F. Devaux, G. Fanjoux, and E. Lantz, Eur. Phys. J. D **28**, 447 (2004).
[11] O. Jedrkiewicz, Y.-K. Jiang, E. Brambilla, A. Gatti, M. Bache, L. A. Lugiato, and P. D. Trapani, Phys. Rev. Lett. **93**, 243601 (2004).
[12] K. Bencheikh, O. Lopez, I. Abram, and J. A. Levenson, Appl. Phys. Lett. **66**, 399 (1995).
[13] E. Lantz and F. Devaux, Eur. Phys. J. D **17**, 93 (2001).
[14] F. Devaux and E. Lantz, Opt. Commun. **114**, 295 (1995).
[15] Y. Jiang, O. Jedrkiewicz, S. Minardi, P. D. Trapani, A. Mosset, E. Lantz, and F. Devaux, Eur. Phys. J. D **22**, 521 (2003).
[16] F. Devaux and E. Lantz, J. Opt. Soc. Am. B **12**, 2245 (1995).